

PREPARED FOR SUBMISSION TO JINST

Design and Performance of the GERDA Low-Background Cryostat for Operation in Water

K. T. Knöpfle and B. Schwingenheuer

*Max-Planck-Institut für Kernphysik,
Saupfercheckweg 1, D-69117 Heidelberg, Germany*

E-mail: Karl-Tasso.Knoepfle@mpi-hd.mpg.de

ABSTRACT: In searching for the neutrinoless double-beta decay of ^{76}Ge the GERmanium Detector Array (GERDA) experiment at the INFN Laboratori Nazionali del Gran Sasso has achieved an unprecedented low background of well below 10^{-3} cts/(keV·kg·yr) in the region of interest. It has taken advantage of the first realization of a novel shielding concept based on a large cryostat filled with a liquid noble gas that is immersed in a water tank. The germanium detectors are operated without encapsulation in liquid argon. Argon and water shield the environmental background from the laboratory and the cryostat construction materials to a negligible level. The same approach has been adopted in the meantime by various experiments. This paper provides an overview of the design and the operation experience of the 64 m^3 liquid argon cryostat and its associated infrastructure. The discussion includes the challenging safety issues associated with the operation of a large cryostat in a water tank.

KEYWORDS: Double-beta decay detectors, detector design and construction technologies and materials, overall mechanics design, cryogenics.

Contents

1	Introduction	2
2	Design consideration for the cryostat - water tank system	4
2.1	Shielding of external γ background	4
2.2	Safety considerations	6
3	Engineering description of cryostat	7
3.1	Layout	7
3.2	Support of inner vessel	9
3.3	Multilayer superinsulation	12
3.4	Additional thermal insulation	12
3.5	Production engineering	13
3.6	The internal copper shield	14
4	Cryogenic infrastructure	15
4.1	Cryogenic piping	16
4.2	Active cooling of LAr	16
4.3	Vacuum system	18
4.4	Pressure regulation	18
4.5	Safety devices against overpressure	18
4.6	Exhaust gas heater	19
4.7	Slow control and graphical user interface	19
4.8	Water drainage	20
5	Specific safety aspects	21
5.1	Evaporation rates in case of failures	21
5.2	Critical operational parameters, alarms and mitigating actions	23
6	Commissioning and Performance	24
6.1	Work at manufacturer	24
6.2	Work in hall A of LNGS	25
6.3	Performance and operating experience	28
7	Conclusion	29
A	Heat transfer to LN2 and LAr in the pool boiling regime	30
B	Timeline of the GERDA experiment	31

1 Introduction

The GERmanium Detector Array (GERDA) collaboration has terminated in February 2020 its search for neutrinoless double-beta ($0\nu\beta\beta$) decay of ^{76}Ge , $^{76}\text{Ge} \rightarrow ^{76}\text{Se} + 2e^-$ [1–7]. Located in hall A of the INFN deep-underground Laboratori Nazionali del Gran Sasso (LNGS), Italy, the experiment used germanium (Ge) diodes fabricated from high purity Ge material enriched in the ^{76}Ge isotope fraction, simultaneously as source and detector. The experimental signature for $0\nu\beta\beta$ decay is the observation of a peak in the energy spectrum of the $2e^-$ final state at the endpoint of the continuous energy spectrum of the standard $2\nu\beta\beta$ double beta decay, $^{76}\text{Ge} \rightarrow ^{76}\text{Se} + 2e^- + 2\bar{\nu}$, which for ^{76}Ge is at the transition energy $Q_{\beta\beta} = 2039 \text{ keV}$. The observation of $0\nu\beta\beta$ decay would have significant implications on particle physics and cosmology: it would establish lepton number violation, and the neutrino to be its own anti-particle (Majorana particle) supporting in this way theoretical explanations of the baryon asymmetry in our universe [8].

When the GERDA experiment was conceived in 2004 [9] previous experiments had shown the detection of this hypothetical process to be extremely demanding. Almost 4 decades after the pioneering investigation into the $0\nu\beta\beta$ decay of ^{76}Ge by the Milano group [10] its half-life limit had been improved by 5 orders of magnitude to about 10^{25} years. Major progress was due to the continuous reduction of the background index (BI) which is the number of events at $Q_{\beta\beta}$ normalized to a 1 keV energy interval and exposure (product of detector mass M and measurement time t). Another big improvement is due to the use of enriched germanium since the signal-to-background ratio scales with the enrichment fraction. However, none of the experiments was ‘background-free’, i.e., had an expected background count < 1 at full exposure within an energy interval given by the energy resolution around $Q_{\beta\beta}$. Hence their lifetime limit improved only as $\sqrt{M \cdot t}$ and not linearly in $(M \cdot t)$ as in the ‘background-free’ case. It was the goal of GERDA to realize for the first time a ‘background-free’ experiment [9].

GERDA achieved this goal in two steps. In Phase I (November 2011 to May 2013), it improved the BI at $Q_{\beta\beta}$ to $10^{-2} \text{ cts}/(\text{keV} \cdot \text{kg} \cdot \text{yr})$, a factor of 10 lower than in previous Ge experiments [2]. After an upgrade [3], Phase II (December 2015 to May 2018 and July 2018 to December 2019) yielded a further reduction of the BI by more than a factor of 10 [4–7]. A value well below $10^{-3} \text{ cts}/(\text{keV} \cdot \text{kg} \cdot \text{yr})$ had never been reached so far by any other $0\nu\beta\beta$ decay experiment if normalized by the energy resolution [7].

Prerequisite for this success was the transition from the traditional compact lead-copper shielding approach to the realization of a novel shielding concept. It emerged from the proposal [11] to operate Ge detectors in ultra-pure liquid nitrogen (LN2) because of the radiopurity of LN2 and its low Z . As we will discuss in the next section, LN2 was replaced by liquid argon (LAr).

Figure 1 shows the GERDA detector array of bare Ge diodes immersed in a large volume (64 m^3) of high purity (N5.0) LAr, which serves both as cooling and shielding medium. For Phase II, the LAr was turned into an active veto system by adding instrumentation for the readout of its scintillation light. The LAr is contained in a vacuum-insulated cryostat of

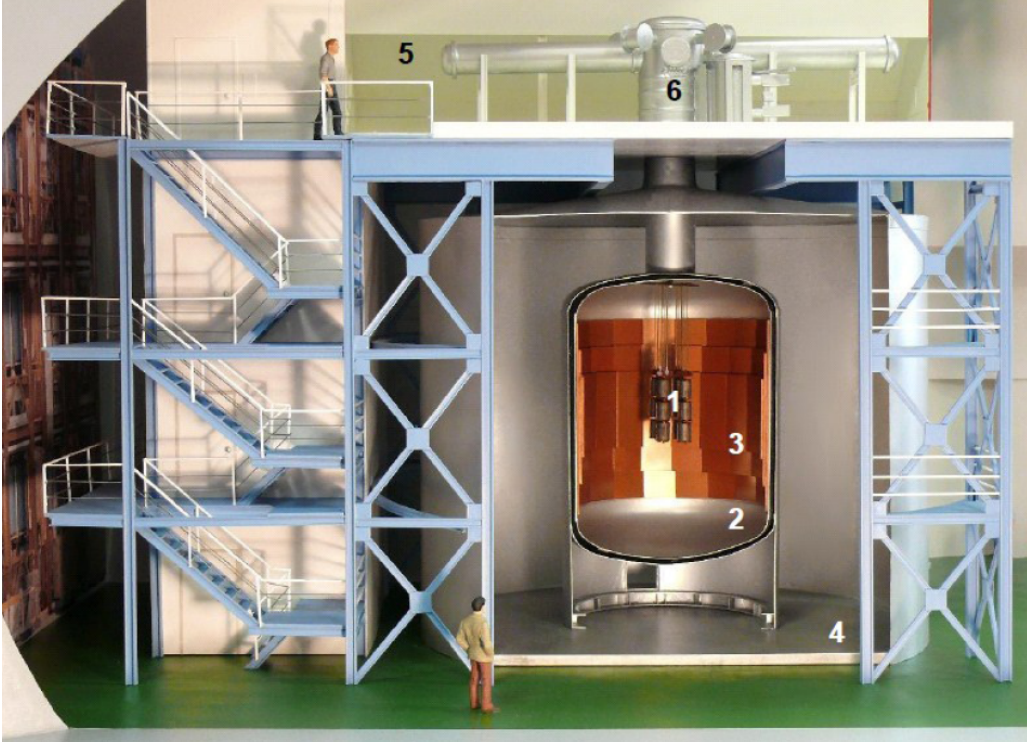


Figure 1. Artist's view of the GERDA experiment in hall A of LNGS showing the (enlarged) germanium detector array (1), the LAr cryostat (2) with internal copper shield (3), the surrounding water tank (4), the clean room (5), and the lock (6) through which the Ge detectors are deployed into the cryostat.

4.2 m diameter which itself is submerged in a large (650 m^3) water tank of 10 m diameter.¹ The purified water ($> 0.17 \text{ M}\Omega\cdot\text{m}$) complements the shielding against the radiation from the surrounding rock and concrete; it serves also as neutron shield and as the medium for an active muon veto system [13].

This installation comprises the first and so far the largest cryostat that is operated underground within a large water tank. The same approach has been adopted in the meantime by various experiments [14–17]. The new scenario of a cryostat immersed in water required to construct a cryostat of extreme reliability. Because the surrounding water represents a huge heat source, the failure/leakage of one of the two or both cryostat shells could result in a huge evaporation or even a rapid phase transition of the cryogenic liquid with potentially severe consequences. Special design features, extensive safety reviews and a first measurement of the heat transfer in LAr contributed to a successful mitigation of the associated risks. Since its first LAr fill in 2009 the cryostat has been operated without any safety problem. Thus a major part of the GERDA experimental setup including cryostat and water tank will be used for the upcoming LEGEND-200 experiment [18].

This paper describes construction and performance of the cryostat including its cryo-

¹A similar setup with LN₂ as cryoliquid had been proposed earlier [12], but has never been realized.

genic system. Section 2 discusses the specific design criteria of the water tank - cryostat system and the associated safety aspects. Section 3 presents the engineering description of the cryostat, section 4 the supporting cryogenic infrastructure. Section 5 addresses special safety aspects of the operation of a cryostat in a water tank. Appendix A provides supplementary material on heat transfer in the pool boiling regime. Section 6 summarizes acceptance tests of the cryostat and its performance. Section 7 concludes the paper. Appendix B shows the timeline of the GERDA experiment in more detail.

2 Design consideration for the cryostat - water tank system

Two major requirements determined the design of the cryostat and the surrounding water tank, (i) reduction of the external γ radiation to the desired level, and (ii) outstanding safe longterm operation. The first issue determines the size of cryostat and surrounding water tank as well as the radio-purity of construction materials, the second - based on rigorous risk analysis - the layout, construction procedures and certification of cryostat and cryogenic infrastructure. Additional constraints include a minimum water thickness of about 2 m to moderate neutrons efficiently and to provide a sufficiently large Cherenkov medium for muon detection. The introduction of the water volume allows to use a smaller volume of cryogenic liquid which is highly desirable from safety aspects. The diameter of the cryostat is also limited by road transport to less than 4.5 m. Last but not least the cryostat - water tank assembly has to fit into the allocated space in hall A, that is within a diameter and height of 10 m, respectively. On top of that, about 2.5 m in height (4 m at center) are left for cleanroom and lock through which the Ge detectors can be deployed directly in the LAr contained in the cryostat (see Fig. 1 and Figs. 2 & 10 in [19]).

2.1 Shielding of external γ background

The external background consists of γ rays from the primordial decay chains, neutrons and muons. As to the γ background at $Q_{\beta\beta}$ the predominant contribution is expected to be due to the Compton tail of the 2.615 MeV γ line of the ^{208}Tl decay. In hall A of LNGS the respective 2.615 MeV flux (surface activity) has been measured to be $(0.031 \pm 0.09)\text{cts}/(\text{s}\cdot\text{cm}^2)$ [20]. Assuming twice this value, measurements and Monte Carlo studies have yielded for the BI of a shielded 2 kg Ge diode in hall A [19] the approximation of $BI = 2250 \cdot X \cdot \exp(-X) \text{cts}/(\text{keV}\cdot\text{kg}\cdot\text{yr})$ where $X = \sum_i (t_i \mu_i) > 5$ is the sum of the products of thickness t_i and linear absorption coefficient μ_i of the various shielding materials i . Table 1 lists absorption coefficients and activities of potential shielding materials. The condition $BI = 10^{-3} \text{cts}/(\text{keV}\cdot\text{kg}\cdot\text{yr})$ yields $X = 17.5$. It implies that the surface activity of hall A of $0.0625 \text{Bq}/\text{cm}^2$ has to be reduced by a factor $\exp(-17.5)$ to $1.6 \text{nBq}/\text{cm}^2$ which yields $t = 563 \text{cm}$ for LN2. Hence, to fit into hall A, a graded shield has to be considered in which part of the LN2 is substituted by materials of larger absorption coefficients and adequate radiopurity (see Table 1). Due to its high radiopurity water is a perfect substitute for LN2.

Figure 2 shows on the left a graded shield of water, copper of $t = 3 \text{cm}$ thickness as construction material for the cryostat, and LN2. The thickness of the water layer is chosen

Table 1. Linear attenuation coefficients μ for 2.615 MeV γ rays in various materials including liquid nitrogen (LN2) and liquid argon (LAr), the material's assumed ^{228}Th mass activity A_m as well as the corresponding surface activity A_s for thickness t (see [19]). Note that, unexpectedly, it was possible to procure stainless steel of significantly lower radioactivity (see Table 3).

materials	μ	ρ	$A_m(^{228}\text{Th})$	$A_s(^{208}\text{Tl})$
	$[\text{cm}^{-1}]$	$[\text{g} / \text{cm}^3]$	$[\mu\text{Bq/kg}]$	$[\mu\text{Bq/cm}^2]$
LN2	0.0311	0.81	*	*
water	0.0427	1.0	1	$t > 1 \text{ m}: 0.01$
LAr	0.050	1.39	*	*
steel	0.299	7.87	$2 \cdot 10^4$	$t = 2 \text{ cm}: 84.5$
Cu	0.338	8.96	25	$t = 3 \text{ cm}: 0.15$
				$t > 16 \text{ cm}: 0.24$
Pb	0.484	11.35	30	$t > 10 \text{ cm}: 0.25$

* negligible

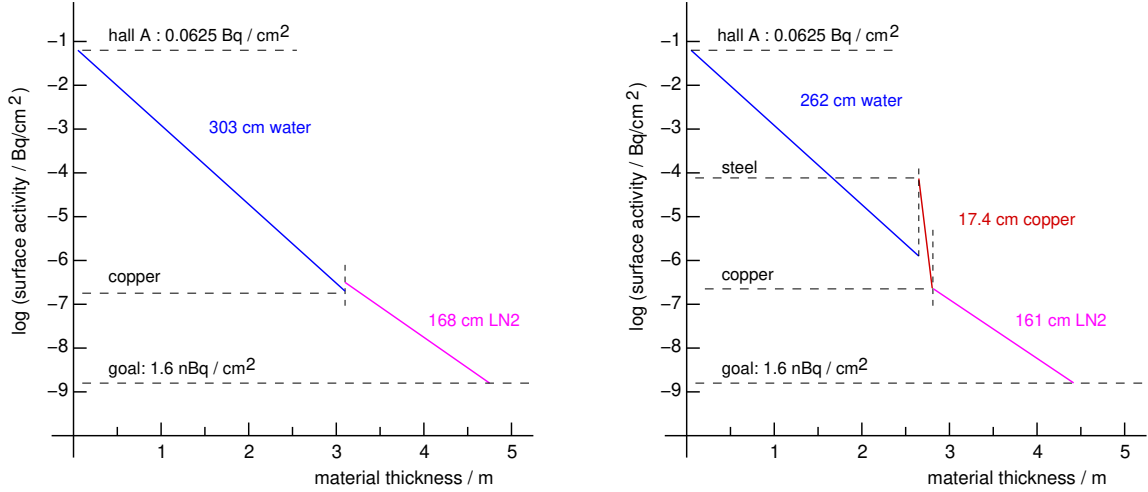


Figure 2. Surface activities as a function of shielding thickness for the graded shields of the GERDA baseline design of a copper cryostat (left) and the alternative of a stainless steel cryostat with an internal copper shield (right). Thicknesses of water, copper and LN2 layers are indicated.

such to attenuate the external 2.615 MeV γ flux to the level of the copper surface activity. To reduce the resulting low surface activity of $0.3 \mu\text{Bq/cm}^2$ to the desired surface activity of 1.6 nBq/cm^2 , the LN2 layer has to be 168 cm thick. Taking the radial extension of the Ge detector array into account, the inner diameter of the cryostat has to be 3.9 m to achieve the desired BI. Preparations for the construction of an electron-beam welded superinsulated cryostat of this size from low-radioactivity OFE copper (^{228}Th activity below $20 \mu\text{Bq/kg}$) were well in progress when an unexpected increase of cost and safety concerns stopped the project.

The alternative design of a cryostat made from stainless steel (^{228}Th activity of 20

mBq/kg, typical for steel used in the Borexino experiment) would require a LN2 layer of 351 cm thickness that, together with the water layer, would not fit into hall A. Even the equivalent thickness of an LAr layer of 217 cm would barely be acceptable and would result in a total diameter that prohibits road transport. An additional copper layer of 17.4 cm thickness will, however, reduce the surface activity of the steel to $0.24 \mu\text{Bq}/\text{cm}^2$ so that a LN2 layer of 161 cm thickness is needed (Fig. 2, r.h.s.). The thickness of the water shield has to be chosen such that it suppresses the external ^{228}Th activity to a fraction of the steel surface activity. For a 1% fraction the required water thickness is 262 cm. In this case, the design of the cryostat has to accommodate also the additional weight of the internal copper shield which is about 50 tons.

The above estimates have been refined by detailed Geant4 simulations with a cryostat geometry very close to that actually built [21]. The neck through which the detector array is deployed has no water shielding which is ignored in above estimates. The full simulation showed however that the γ flux through the neck is dominating the background for LN2 filling. This result together with the advantage of a reduced Cu thickness for LAr and the additional background suppression by the detection of argon scintillation light led to the decision to drop the LN2 option. The final solution is a double-walled superinsulated stainless steel cryostat of cylindrical shape with an internal copper shield and a 172 cm long neck (see next section). With a LAr fill the surrounding ^{228}Th radioactivity is expected to contribute $8 \cdot 10^{-6} \text{cts}/(\text{keV}\cdot\text{kg}\cdot\text{yr})$ to the BI [21].

2.2 Safety considerations

The storage of a large amount of cryoliquid underground implies the risk to create large volumes of N_2 or Ar gas in case of leakage which themselves are not poisonous but might cause suffocation of people working in the underground area. The standard mitigation of this risk is monitoring the O_2 content in air, and increased ventilation in case of too low O_2 concentration. The operation of a cryostat in water constitutes an enhanced risk since leakage would imply here both the possibility of a fast evaporation of the cryoliquid or the mixing of water and LN2/LAr resulting in an even faster possibly explosive phase transition. Hence it is obvious that the risk of leakage should be minimized, as much as possible, by design and construction. These measures are summarized below while the mitigation of leakage and the safety aspects of the whole system are discussed in section 5.

The design and production of the cryostat have been done according to the European Pressure Equipment Directive (PED 97/23/EC) for a nominal overpressure of $1.5 \cdot 10^5 \text{ Pa}$, even though it is operated at $0.3 \cdot 10^5 \text{ Pa}$ and hence below the limit of $0.5 \cdot 10^5 \text{ Pa}$ above which this code applies. An additional safety margin is achieved by the increase of 3 mm of the wall thickness of the inner (cold) vessel which allows its evacuation. Evacuation is needed for He leak tests, Rn emanation measurements and, before the filling with LAr, the removal of contaminations. No ports below the filling levels of cryoliquid and water have been implemented. Standard cryostats have ports e.g. at the bottom for emptying or for measuring the hydrostatic pressure which are known [22, 23] to increase the risk of leakage. The entire cryostat is rotational symmetric so that local stress is minimized. Where this symmetry is broken locally, i.e. at the location of the support and centering

pads, the wall thickness is enlarged to lower absolute stress values. Different from standard cryostats where the inner cold vessel is hung at the neck, it is resting here on pads at the bottom. This reduces stress peaks from loads due to earthquakes. In fact, the cryostat is designed to withstand loads from the ‘Maximum Credible Earthquake’ [24] of up to 0.6 g horizontally and vertically without damage. The use of highly ductile stainless steel as exclusive construction material enforces the ‘leak-before-break’ concept [25]. The choice of a stainless steel alloy with Mo and Ti additions, 1.4571 (X6CrNiMoTi17-12-2), warrants improved corrosion resistance. The inspections or certifications specified by the PED guarantee a high production quality that is enhanced by the special requirement of 100% X-ray inspection of the accessible welds.

3 Engineering description of cryostat

3.1 Layout

Views of the cross section and a solid model of the cryostat² are shown in Fig. 3 and Fig. 4; its main characteristics are listed in Table 2.

The cryostat³ consists of two coaxial vessels that are built from torospherical heads⁴ of 3976 mm and 4160 mm inner diameter and corresponding cylindrical shells of 3900 mm and 4149 mm height. Each vessel has a cylindrical neck of 789 mm and 964 mm inner diameter, respectively, and of about 1.7 m height; on top they are connected to each other by a flange which will hold a full metal seal. Since the inner container rests via pads on the bottom of the outer vessel (see below), its shrinkage of about 2 cm when cooled down from 300 K to 77(88) K is compensated by a double-walled stainless steel expansion joint⁵ in its neck. It is kept centered by six Torlon[®] spacers within the neck and at the bottom. In case of earthquake the largest stress will occur at the transition between neck and upper vessel head, and thus this part is reinforced by an additional stiffening ring.

The volume between inner and outer vessel, about 8 m³, will hold the vacuum multi-layer insulation. Access to this volume is provided by four CF200 flanges at the very top of the neck which are used as connections to the pumping station, safety and pressure relieve valves and manometers (see Fig. 4). The flanges are separated from the water tank by a circular collar around the neck that represents also the support ring for the flexible fabric which closes the gap between cryostat and water tank.

The inner (cold) vessel is designed for vacuum and $1.5 \cdot 10^5$ Pa overpressure (i.e. $2.5 \cdot 10^5$ Pa absolute pressure) together with the hydrostatic pressure of LAr. The outer vessel is designed for $1.0 \cdot 10^5$ Pa overpressure and vacuum together with an external pressure of a water column of 7.8 m ($-1.78 \cdot 10^5$ Pa external overpressure). The construction material, type 1.4571 stainless steel, purchased in various batches of varying thickness for vessel

²An alternative layout based on an available standard cryostat design has been provided by PJSC “Cryogenmash” 143907, Balashikha, Moscow Region, Russia.

³Fabricated by Simic S.p.A., I-12072 Camerana, Italy.

⁴Produced by ANTONIUS, NL-6051 Al Maasbracht, The Netherlands.

⁵Delivered by HKS Unternehmensgruppe, D-18057 Rostock, Germany.

Table 2. Characteristics of cryostat.

Materials, Th-228 radiopurity		
vessels, compensators	1.4571* (25 ton)	0.1-5 mBq/kg
multilayer insulation	alu. polyester (15 kg)	<10 mBq/kg
support/centering pads	Torlon [®] (8 × 2.6 kg)	<5 mBq/kg
Belleville springs	Inconel X718 (8 × 4.2 kg)	not avail.
internal shield	OFRP copper (16 ton)	20 μ Bq/kg
Geometry		
overall height × diameter	8.89×4.20	[m]
neck height × inner diameter	1.72×0.80	[m]
nominal volume	64	[m ³]
wall thickness inner vessel	12, 15	[mm]
wall thickness outer vessel	12, 18, 20	[mm]
volume bet. inner & outer vessel	8	[m ³]
LAr fill level	6.81	[m]
Masses		
empty vessel	25	[ton]
max. load inner vessel LAr/Cu	90 / 48	[ton]
Pressures		
inner vessel max./min. pressure**	1.5 / -1.	[10 ⁵ Pa]
outer vessel max./min. pressure**	1.0 / -1.78	[10 ⁵ Pa]
Multilayer insulation		
number of layers	30	
thermal loss	<300	[W]
active cooling power	500	[W]
Construction code	AD2000, DGRL 97/23/EC , cat IV, mod G	
fraction of x-rayed welds	100%, final orb. weld except	
Earth-quake tolerance	0.6g hor. & vert.	

* X6CrNiMoTi17-12-2

** relative to atmospheric pressure

heads and cylindrical walls, has been screened by γ spectroscopy [26], and the results for the crucial ²²⁸Th activity are shown in Table 3.

A cylindrical skirt made from 12 mm thick stainless steel holds the cryostat 1280 mm above floor. Two manholes provide access to the volume underneath the cryostat, and 8 circular ports allow this volume to be watched by photomultipliers of the muon veto system [13]. The bottom of the skirt is reinforced with an annular structure by which the cryostat is attached to the floor with 24 M39 stainless steel bolts arranged equidistantly on a bolt circle of 4 m diameter.

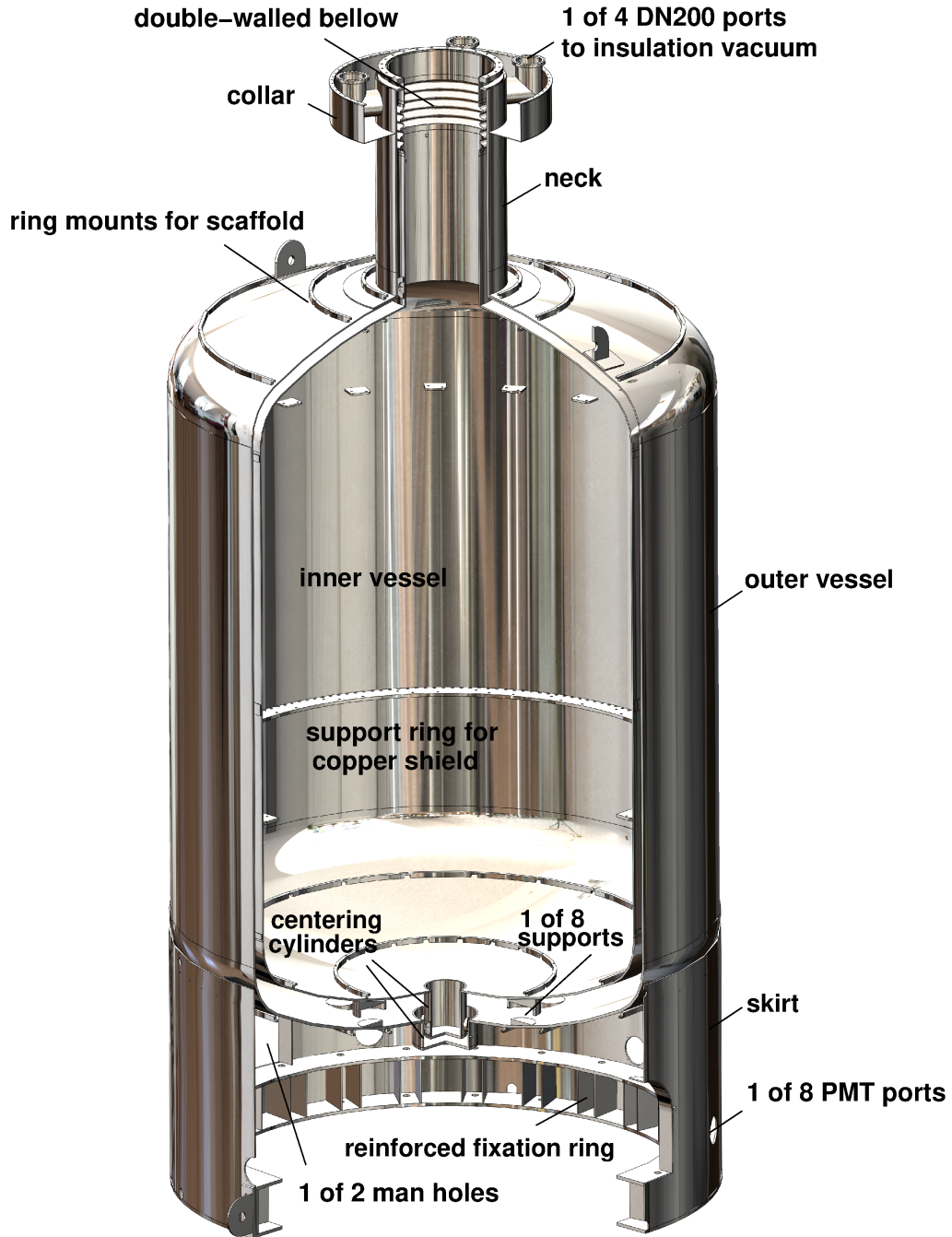


Figure 4. CAD drawing of the steel parts of the GERDA cryostat.

support pad. The usual material for support pads, glass fiber reinforced epoxy, has been replaced by tubes ($\varnothing 183(100) \times H 100$ mm) made from Torlon[®] 4203/4503. At 77 (296) K this polyamide-imide (PAI) material exhibits a better radiopurity of <14 mBq/kg (^{228}Th), a lower thermal conductivity of 0.1 (0.26) W/(m·K [27]), and comparable flexural strength

Table 3. Size and activity (in mBq/kg) of 1.4571 stainless steel sheet material used for vessel production. Full screening information is provided for each sample in [26].

Outer vessel	Sample	L x H x t [mm ³]	²²⁸ Th	⁶⁰ Co
top head	D3	4800 x 2500 x 12	1 ± 0.4	15
	D3	4800 x 2500 x 12	1 ± 0.4	15
wall	G5	6000 x 2000 x 20	1.5 ± 0.2	16
	G1	1900 x 2000 x 20	< 0.2	46
	D6	6000 x 2000 x 20	< 0.8	17
	G1	6000 x 2500 x 20	< 0.2	46
	G2	8000 x 2500 x 20	< 0.1	14
bottom head	D1	4800 x 2500 x 20	3.4 ± 1	7
	D1	4800 x 2500 x 20	3.4 ± 1	7
Inner vessel				
top head	D2	4600 x 2500 x 12	< 1.7	14
	D2	4600 x 2500 x 12	< 1.7	14
wall	G3	12900 x 2000 x 12	< 0.4	14
	G3	12900 x 2000 x 12	< 0.4	14
bottom head	D5	4600 x 2500 x 15	< 1.1	17
	D4	4600 x 2500 x 15	< 1.8	15

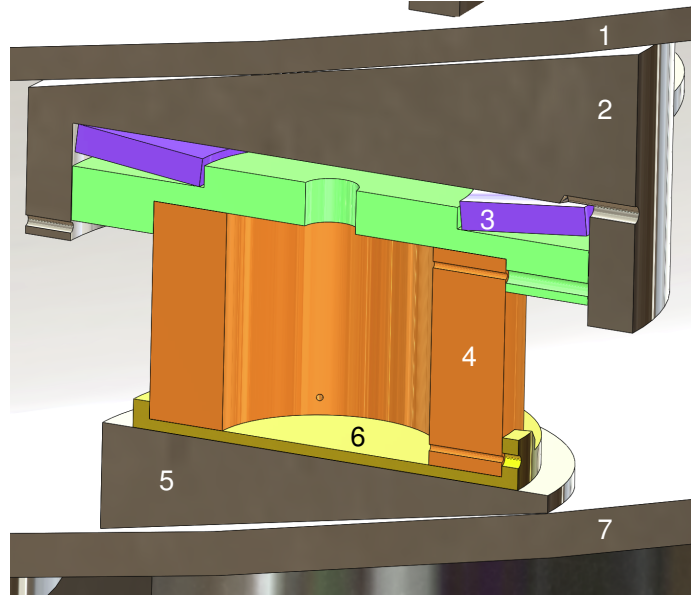


Figure 5. Close up of one of the eight supports on the bottom of the inner vessel consisting of the cage (2) for the Belleville spring (3) welded to the bottom vessel head of the inner vessel (1), the Torlon[®] cylinder (4) for thermal insulation, and the countersurface (5) at the bottom vessel head (7) of the outer vessel. The bronze shoe (6) for improved sliding has not been implemented.

of 282 (244) MPa [28]). Belleville springs⁶ made from Inconel X718 with spring constants

⁶Delivered by MUBEA, D-57567 Daaden, Germany.

of 58 kN/mm are used to compensate small differences of the gaps between the bearings so that all pads will carry about equal load once the cryostat is filled (see sect. 6.1). Each pad is fixed at the cold inner vessel. During cool down, the warm end of the pad will move by about 3 mm.

3.3 Multilayer superinsulation

The complete outer surface of the inner vessel is covered up to the compensator with multilayer superinsulation (MLI) consisting out of 2x 15 layers.⁷ The nominal thickness of a 15 layers MLI blanket is 3 to 5 mm. The inner and outer layers of a blanket are made from TERIL 53, a 6 μm thick polyester film aluminized on both sides with a thickness of 400 Å, reinforced with a polyester net. The other 13 layers consist of IR 305, i.e. a 6 μm thick perforated polyester film aluminized on both sides with a thickness of 400 Å, and a polyester tulle with an approximate weight of 5 g/m². The perforation diameter is 2 mm, and the distance between perforations is 56 mm. Fig. 6 shows the bottom part of the inner vessel including the Torlon[®] pads with the MLI assembly. Table 4 shows that the 8



Figure 6. Detail of the MLI arrangement at the bottom of the inner vessel showing the coverage of support and centering pads.

Torlon[®] pads and the superinsulation contribute similarly to the expected thermal loss of about 250 W while the neck - due to its thin walled (2x 0.8 mm thick) bellow - contributes 10% only.

3.4 Additional thermal insulation

Inner and outer vessel carry thermal shields which keep the Ar evaporation rate below 10⁴ m³/h (STP) for the case of a water/LAr leak in the outer/inner vessel (see section 5).

⁷Delivered and mounted by Jehier, F-49120 Chemille, France.

Table 4. Contribution of various components to thermal losses.

Component	area, height	thermal conductivity	thermal loss
neck, bellow	0.0041 m ² , 0.44 m	15 W/(m·K)	30 W
Torlon [®] pads	8x0.041 m ² , 0.1 m	0.18 W/(m·K)	128 W
superinsulation	100 m ² , -	0.5 W/m ²	100 W*

* including safety factor of 2

The outside surface of the vertical shell of the inner vessel is covered below the MLI with a 6 mm thick polycarbonate (Makrolon[®]). This material has been chosen since its properties are adequate for the use at cryogenic temperatures, and since it is rigid and has a relatively low thermal conduction coefficient of 0.2 W/(m·K). Less favourable features are its relatively large linear thermal expansion coefficient ($65 \cdot 10^{-6}/\text{K}$ at room temperature) as well as its water absorption of 0.12% at 23 °C and 50% relative humidity.

Similarly, the outer surface of the vertical shell of the outer vessel as well as its bottom are covered with 6 mm thick extruded polystyrol foam⁸ which is hermetically covered by a multilayer polyester foil⁹ with > 98 % specular reflectance that serves in addition as reflector for the Cherenkov radiation in the water tank.

The thickness of the polycarbonate and the polystyrol layers have been deduced from test measurements of the heat transfer in the pool boiling regime for the interface liquid nitrogen - stainless steel - water (see section 5).

3.5 Production engineering

The production process was subject to the AD 2000 code and PED 97/23/EG and controlled by representatives of a notified body (TÜV Nord, Germany). We summarize here a few non-standard additional features for further improvement of the cryostat's reliability and performance.

The production of the cryostat and the MLI installation have been carried out in a 'gray' area which was separated from the standard carbon steel production sites. All welds were done by TIG welding using exclusively thorium-free TIG-welding electrodes. For the welding filler, material of less than 5 mBq/kg ²²⁸Th radioactivity has been selected. Before production, the effectiveness of weld preparation and procedures even in case of thermal shocks was verified with two 500 mm long 1.4571 sheets that were welded together and subsequently immersed into liquid nitrogen. The chosen welding procedure yielded for the low temperature notch impact energy the value of 120 J that is almost 4 times higher than required by AD2000. All welds have been passivated to avoid corrosion. The cleaning procedure for all inner and outer surfaces included removal of oil and grease, pickling and passivation, rinsing with de-ionized water and subsequent drying. Ferroxy tests did not reveal any ferrite inclusions on the surfaces.

⁸ Jackodur KF300 FTD by JACKON Insulation GmbH, D-33803 Steinhagen, Germany.

⁹ VM2000 by 3MTM Deutschland GmbH, D-41453 Neuss, Germany.

All accessible welds of the inner and outer container of the cryostat have been 100% X-ray tested. Where such a test was not possible like at the final orbital weld an ultrasonic test was done.

3.6 The internal copper shield

The screening of the stainless steel material used for the cryostat yielded an unexpected low radioactivity [26] that allowed to reduce the amount of the internal copper shield from the envisaged 48 tons to less than 16 tons. Its thickness and profile have been determined by Monte Carlo calculations [21]. The profile is symmetric w.r.t. the midplane, the thickness is 6 cm up to the height of 1 m, and continues from there with 3 cm thickness up to 1.4 m (see Fig. 7). The shield is assembled from 20 overlapping segments which fit through the cryostat's neck. Each segment consists of three 3 cm thick and 61.5 cm wide copper plates of 40, 200 and 240 cm length, respectively. The two longer plates are screwed together and rest on a support ring within the cryostat. The short plate is attached below.

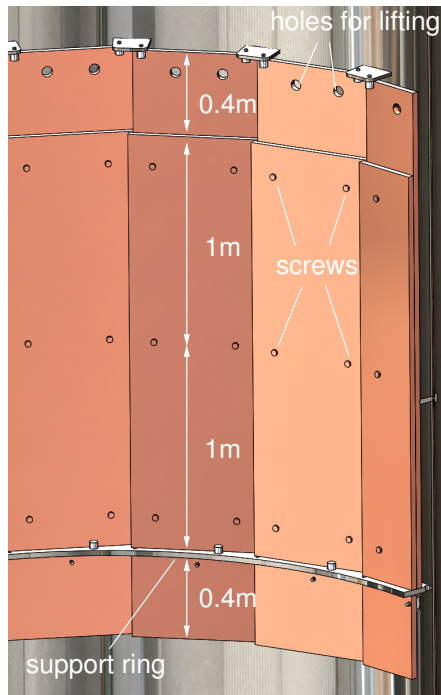


Figure 7. Three (and a half) of 20 segments of the internal copper shield as mounted in the cryostat.

The copper plates have been rolled¹⁰ in spring 2007 from freshly produced OFPR copper.¹¹ After rolling, the plates were warmed up to 50° C, pickled in >15% sulfuric acid, and, immediately afterwards, rinsed with de-ionized water. The individual segments were vacuum-packaged after assembly, and an additional plastic wrap protected them for

¹⁰By CSN Schreiber, D-57290 Neunkirchen, Germany.

¹¹By Norddeutsche Affinerie, now Aurubis AG, D-20539 Hamburg, Germany.

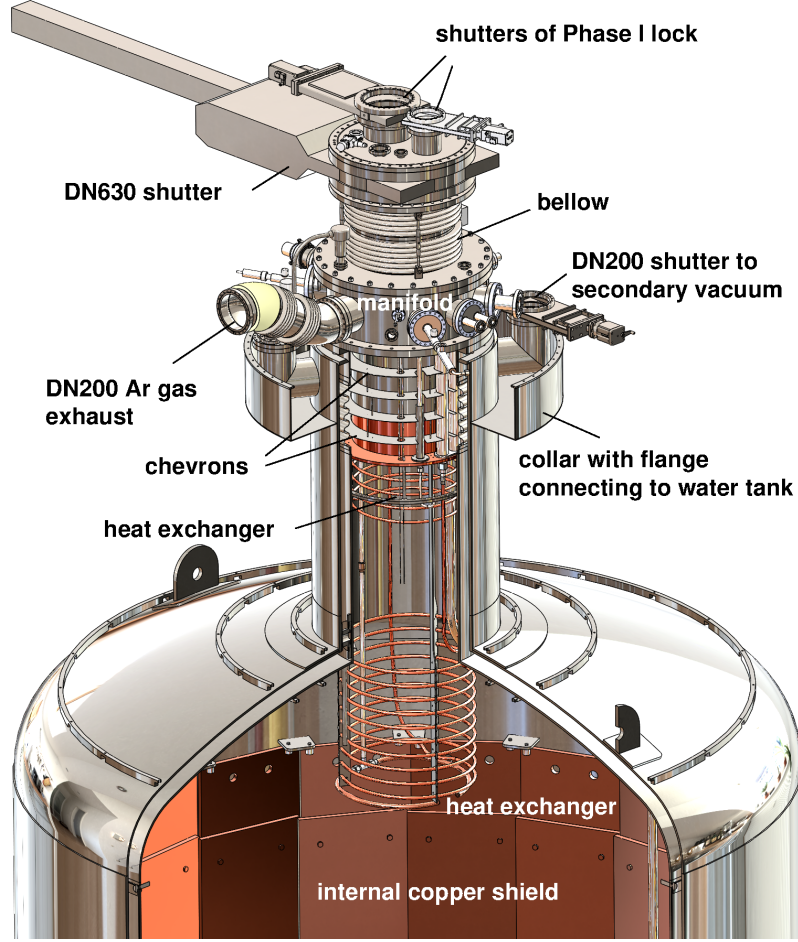


Figure 8. Close up of the top of the cryostat including neck, manifold and interface to the lock. For GERDA Phase II, the two shutters of the Phase I lock above the DN630 shutter have been removed.

transportation to LNGS where they are kept underground since June 2007 to prevent further cosmic activation.

4 Cryogenic infrastructure

The cryogenic infrastructure has to ensure a stable and safe operation of the cryostat. Since the neck provides the only access to the interior of the cryostat, a manifold on top of the neck carries the flanges for all lines that penetrate into the cold volume including filling tube, gas exhaust tube, tubes for active cooling, and feedthroughs for the cryostat instrumentation (see Fig. 8). The manifold is connected with a bellows to a DN630 shutter¹² which is located at the floor of the clean room. The bellows allows for 25 mm lateral movements of the clean room with respect to the cryostat in case of an earth quake. The shutter separates the cryostat from the lock. It is closed while the lock is open for

¹²Gate valve, Series 19, by VAT Deutschland, D-01109 Dresden, Germany.

germanium detector installation. All valves¹³ have metallic sealing against atmosphere. The control of most pneumatic valves and readout of sensors is done with a programmable logic controller (PLC) Simatic S7¹⁴ that is dedicated to the control and monitoring of the cryogenic infrastructure. The power for the entire infrastructure is connected to an uninterruptible power supply backed by a generator which is either driven by normal electric power or a battery.

The various parts of the cryogenic infrastructure are discussed below.

4.1 Cryogenic piping

The first filling of the cryostat with LAr and the optional refilling during the standard operation is done from a selected storage tank (radon emanation about 5 mBq, operated at $3 \cdot 10^5$ Pa) which is located in the TIR tunnel, about 30 m away from the cryostat. At the same location are also 2 storage tanks for LN2. One ($4.0\text{--}4.5 \cdot 10^5$ Pa) for LN2 extraction at the nominal pressure of $3.2 \cdot 10^5$ Pa relative to atmospheric pressure for the LAr active cooling and one for gaseous nitrogen at a higher pressure of $8 \cdot 10^5$ Pa which is used for flushing of glove boxes and the operation of pneumatic valves. For the pipe¹⁵ from the storage tank to the cryostat a triaxial pipe was chosen: the LAr pipe is the inner pipe (DN 25) at a LAr boiling temperature of ≈ 99 K, the LN2 flows outside the LAr pipe in a DN 50 pipe at a lower temperature of ≈ 91.3 K and the space between the DN 50 and the outer third pipe (DN 100) holds the vacuum insulation. The lower LN2 temperature allows to subcool LAr without freezing it (84 K) and hence to reduce argon flash gas losses.

As a safety feature the pressure in the LN2 pipe is used to operate pneumatic valves at the outlets of the storage tanks. If due to a rupture of the pipe, for example, the pressure is too low the valves close and the spilling of LN2 and/or LAr will be stopped.

The LAr passes optionally through a charcoal filter to retain radon (about 1 kg mass) which is cooled with LN2 to about 86 K. Afterwards two PTFE filters¹⁶ with 50 nm pore size and 10 inch length are added in series to retain any particles.

The filters together with all valves for LN2 and LAr are in a vacuum insulated box called ‘valve box’.

Before the LN2 pipe enters the valve box a phase separator called ‘keep cold device’ allows to remove gaseous nitrogen.

4.2 Active cooling of LAr

Inside the cryostat are two LN2/LAr heat exchangers in form of spirals made from 18 mm x 1 mm copper pipes: one at the liquid/gas surface and one in the main volume of the cryostat (see Fig. 8). The diameter of the spirals is about 760 mm.

¹³Cryogenic valves by Flowserve Kammer, D-25524 Itzehoe, Germany; for gases manual valves series BG by Swagelok, Solon, Ohio 44139, USA.

¹⁴Simatic S7 by Siemens, D-80333 Munchen, Germany.

¹⁵Cryogenic piping, ‘valve box’ and ‘keep cold device’ produced and installed by DEMACO, NL-1723 ZG Noord-Scharwoude, The Netherlands.

¹⁶Fluorogard CTFZ01TPE by Entegris Eastern and Central Europe, D-01109 Dresden, Germany.

The pressure at the gas outlet of the heat exchanger is about $1.2 \cdot 10^5$ Pa absolute which corresponds to a LN2 boiling temperature of 79.6 K. The cryostat pressure is also regulated to $1.2 \cdot 10^5$ Pa absolute which corresponds to an LAr boiling temperature of 89.0 K at the liquid surface. Due to the hydrostatic pressure the boiling point increases deeper inside the cryostat. The LAr is cooled to about 88.8 K.

GERDA cryostat Temperature

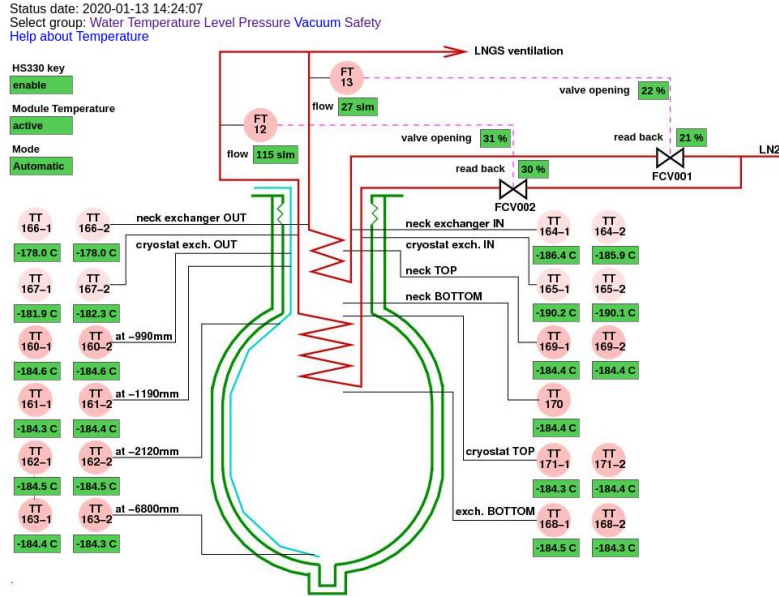


Figure 9. Distribution of temperatures within the LAr cryostat with powered Ge detector array.

There are in total 29 PT-100 sensors inside the cryostat to measure the LN2 temperatures at the heat exchanger inlets and outlets as well as the LAr temperatures at different heights. It turns out (see Fig. 9) that the LAr temperatures are within the precision of our measurement (0.1°C) the same everywhere except at the surface where they can be adjusted to be a few tenths of a degree higher. The interpretation is that convective currents lead to a strong mixing effect and hence to a homogeneous temperature. Also: no argon ice formation at the heat exchangers is observed despite the fact that the LN2 boiling temperature is about 3 degrees below the freezing point.

The LN2 flow regulating valves are inside the valve box. The pressure at the inlet is $3.5\text{--}4 \cdot 10^5$ Pa absolute. After the valves the pressure is only $1.2 \cdot 10^5$ Pa absolute. Because of the pressure drop a gas/liquid mixture passes through the heat exchangers. The diameter of the pipe from the valve box to the cryostat was chosen to be only 8 mm and the pipe is always inclining upwards to ensure a large flow speed such that the gas/liquid mixture does not separate. This concept [29] is supposed to reduce flow variations in the cooling and hence microphonics although the measured gas flow still shows variations by $\pm 20\%$ on a time scale of minutes. Through the bottom heat exchanger the flow is adjusted to on average 120 slm (liters of gas per minute at standard pressure and temperature) and for

the other one to 15 slm.

4.3 Vacuum system

The insulation vacuum is pumped by a 600 ℓ /s turbomolecular pump¹⁷ with mechanical rotor suspension that was backed at full gas load by a 40 m³/h , and later by a 8.5 m³/h rotary vane pump. The pump is mounted with a DN160/200CF adaptor onto a DN200CF shutter¹⁸ that is attached to one of the four CF200 ports (see Fig. 8). After some years of operation the turbomolecular pump was replaced by the smaller 150 ℓ /s model. The turbo pump is running continuously. If momentarily switched off, the pressure increases at $5 \cdot 10^{-7}$ hPa· ℓ /sec.

The pressure is monitored redundantly and read out by the PLC. If it is too high or if, e.g. the turbo pump signals an error, the shutter between cryostat and turbo pump will be closed. The vacuum is also monitored by a residual gas analyzer.¹⁹ The partial pressures for water, argon and nitrogen are read out and can be used to diagnose a problem in case the total pressure rises unexpectedly.

Another one of the four CF200 ports carries the overpressure protection device for the insulation vacuum volume. It is realized by a DN 100 disk with a rubber O-ring seal which is tightened by the air pressure.

4.4 Pressure regulation

The Ar gas pressure in the cryostat is one of the critical parameters. It is regulated by two intelligent pressure transmitters that include a PID (proportional, integral, differential) controller with a mean time between failure (MTBF) of 244 years.²⁰ Each of the analog output signals is directly used to control a DN 50 valve²¹ ($k_{vs} = 40$). These pressure regulation circuits operate therefore independently of the PLC which has a lower MTBF rating.

In case of power failure the above mentioned valves are normally closed. Therefore a DN10 valve²² with a smaller opening ($k_{vs} = 1.6$) was added. The discharge rate through this ‘normally open’ valve is large enough to keep the pressure below $1.2 \cdot 10^5$ Pa absolute for at least one week in case of loss of power or loss of nitrogen for the actuator.

4.5 Safety devices against overpressure

The cryostat is equipped redundantly with a safety valve and a rupture disk. The safety valve²³ has a trigger point of $0.85 \cdot 10^5$ Pa relative to atmospheric pressure and a flow area of 7500 mm². Since the safety valve is not leak tight against the atmosphere, a DN150 rupture disk²⁴ with a trigger point of $0.8 \cdot 10^5$ Pa relative to atmospheric pressure has been

¹⁷Turbovac 600C by Oerlikon Leybold Vacuum, D-50968 Köln, Germany.

¹⁸UHV gate valve, series 10, by VAT Deutschland, D- 01109 Dresden, Germany.

¹⁹Model PPM100 Partial Pressure Monitor by Stanford Research Systems.

²⁰Model LD301 by Smar Europe B.V., D-55545 Kreuznach, Germany.

²¹Type 2415 P3 from Flowserve Kämmer, D-45145 Essen, Germany.

²²Type 241 H3 from Flowserve Kämmer, D-45145 Essen, Germany.

²³Type 411 from LESER GmbH & Co. KG, D-20537 Hamburg.

²⁴Type CF160-UKB-LS-FL 6 from REMBE GmbH Safety + Control, D-59929 Brilon.

added in front. This disk is welded into its stainless steel holder and has ConFlat flange DN160 connections.

The same type is used as rupture disk, here with a maximum trigger point of $1.4 \cdot 10^5$ Pa relative to atmospheric pressure. To signal its rupture or damage a signal rupture disk is added afterwards.

Both devices are large enough to cope with a maximum discharge rate of 4.5 kg/s of argon gas.

4.6 Exhaust gas heater

The argon exhaust gas is passed to the LNGS ventilation system that pushes it through a pipe in the highway tunnel to the outside. In case of a faulty operation of the cryostat the cold argon gas would freeze the water vapor present in the pipe and the fans could stop working. Both scenarios would result in a collapse of the system. The argon gas must therefore be warmed up above 0°C before it is discharged to the LNGS ventilation system. A water/gas heat exchanger²⁵ is installed for this purpose. The exhaust gas from the safety valve and rupture disk of the cryostat, from the safety disk of the insulation vacuum and all other valves is collected into a DN200 pipe which is connected to the inlet of the heat exchanger. The gas then passes through a bundle of 121 pipes with 18 mm inner diameter. Outside the pipes is water to heat up the cold gas. The outlet of the heat exchanger is directly connected to the ventilation system of LNGS. A bypass between inlet and outlet is added with a burst disk to avoid overpressure in case the heat exchanger is blocked for some reason.

The water is normally the cooling water of LNGS but as a backup a pump is installed to pump the water from the water tank through the heat exchanger.

4.7 Slow control and graphical user interface

Apart from the redundant high-reliability pressure regulation, all sensors, valves and pumps of the cryogenic infrastructure are monitored and controlled continuously by the Simatic S7 PLC. The PLC evaluates the safety status of the cryogenic system, and automatically triggers appropriate actions if needed. The safety relevant status information is shared with the LNGS safety network via MODBUS and hardwired by a cable transmitting the relevant status bits. Using CGI scripts, a Linux web server reads or writes data from or to the PLC via TCP/IP access, acting both as DBclient for the general GERDA slow control system [30] and the Hypertext Transfer Protocol (HTTP). Thus performance and status of the GERDA cryogenic system can be examined and, in part, controlled remotely. Fig. 10 shows for example the safety summary page where all critical operation parameters for the cryostat and supporting infrastructure are displayed and color-coded (see subsection 5.2). Other pages show the status of the water system, the temperature distribution (see Fig. 9), the fill level, and the values of the pressures measured for cryostat and insulation vacuum.

²⁵Model C300 1708-2PASS by FUNKE Wärmetauscher Apparatebau GmbH, D-31028 Gronau, Germany.

GERDA cryostat Safety

Status date: 2016-08-12 14:05:28

Select group: Water Temperature Level Pressure Vacuum Safety

Help about Safety

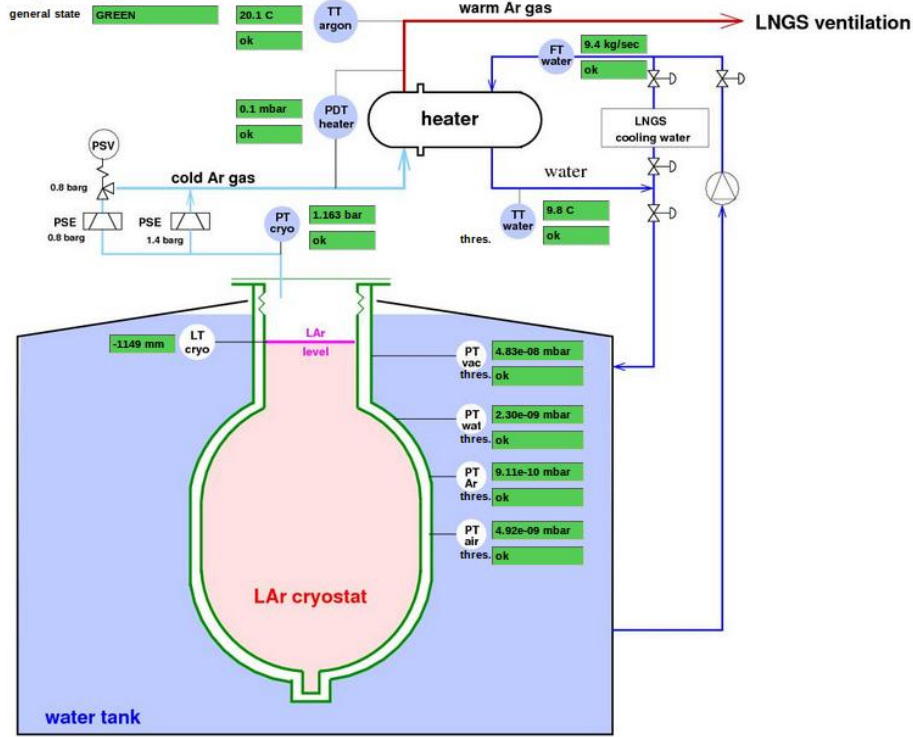


Figure 10. Safety status of the GERDA experiment as inquired at 14:05 on August 8, 2016 via the web interface. The values of all critical operation parameters are within the specifications for standard operation (see subsection 5.2).

4.8 Water drainage

The fast drainage of the water is important in case of an emergency. Therefore the PLC that monitors the cryostat is also controlling the drainage valves of the water tank. There are three different lines: (i) the main DN250 pipe below the tunnel road with an allowed maximum flow rate of $80 \ell / s$, (ii) a DN90 line ($18 \ell / s$) to 100 m^3 storage containers in hall A, the so-called ‘GNO pits’, and (iii) a DN80 pipe ($20 \ell / s$) which is part of the emergency water supply system for the GERDA exhaust heater leading also to the GNO pits. The PLC controls the valves to these lines as well as the flow rate in the main DN250 pipe via a butterfly valve so that a constant standard flow rate of $20 \ell / s$ or, in emergency, a maximum flow rate of $\leq 80 \ell / s$ are maintained independent of the hydrostatic pressure in the water tank.

A test of the fully automated drainage procedure in 2010 showed that measured and predicted drainage times are in very good agreement with each other, and that in case of emergency the water tank can be emptied in less than 2 hours.

5 Specific safety aspects

5.1 Evaporation rates in case of failures

Compared to standard cryogenic installations the GERDA cryostat-water-tank system exhibits the additional risk that the separation between water and the cryogenic container is broken resulting in potentially huge gas exhaust rates.

In the worst case scenario, i.e. the simultaneous rupture of inner and outer container wall, the mixing of LAr and water could lead to a rapid phase transition. External consultants²⁶ have evaluated this risk and found it to be extremely unlikely, $< 10^{-8}$ ev/yr, due to (i) the mutual independence of the two stainless steel cryogenic vessels that are built according to established construction codes, (ii) the irrelevance of corrosion related to the galvanic interaction between copper shield and the austenitic 1.4571 stainless steel, (iii) the earthquake tolerance of 0.6 g, (iv) the redundant monitoring of the critical operational parameters (COPs, see below sect. 5.2), and last but not least, (v) the fulfillment of the ‘leak-before-break’ principle.

In case of a small leak in one of the two vessels the insulation vacuum would be lost. A compilation of the thermal conductivity of superinsulation in dependence of the gas pressure shows [31] that in the most conservative estimate a superinsulation with a heat flux of 1 W/m^2 between 77 and 300 K is degraded by a factor of 1000 in case of a complete loss of insulation vacuum. Hence, with the cryostat’s surface of about 100 m^2 and 97 tons of LAr it will take about 44 hours until all LAr has been evaporated. The resulting gas flow (20°C) of about $1340 \text{ m}^3/\text{h}$ is small compared to the limit of $10000 \text{ m}^3/\text{h}$ set by LNGs.

A major leak in the outer vessels would destroy not only the insulation vacuum but enable the surrounding water to enter the space between inner and outer vessel. Water with its high specific heat capacity of $4.19 \text{ kJ}/(\text{kg}\cdot\text{K})$ represents an efficient heater for the cryogenic liquid. A drop of less than 6°C in temperature of the 590 m^3 stored water is enough to evaporate the 64 m^3 of LAr contained in the cryostat. An estimate of the resulting gas flow is difficult lacking detailed knowledge of the involved heat transfer. The heat transfer in an unsteady state involving phase changes has been discussed by various authors, see e.g. [32, 33] but the application of the reported results is not obvious. Hence, experimental model studies have been performed in order to arrive at a more quantitative understanding of the evaporation rates in a worst case scenario for a water-cryostat system (see Appendix A).

Using the deduced maximum heat transfer coefficient of 27 kW/m^2 for LAr, the rate of exhaust gas for the GERDA configuration with a total mass of 90 tons of LAr is predicted for the worst case scenario, that is the sudden removal of the outer container such that the inner cryogenic container is immediately exposed to the surrounding water. The black circles in Fig. 11 show that at the assumed heat transfer coefficient of 27 kW/m^2 the total mass is evaporated after less than 5 h, and that the corresponding gas exhaust rate peaks at almost $30000 \text{ m}^3/\text{h}$ which is not acceptable. However, if the heat transfer through the cylindrical wall is limited to 5 kW/m^2 (red curves in Fig. 11) it will take about 9

²⁶Nier Ingegneria S.p.A., I-40013 Castel Maggiore (Bo), Italy.

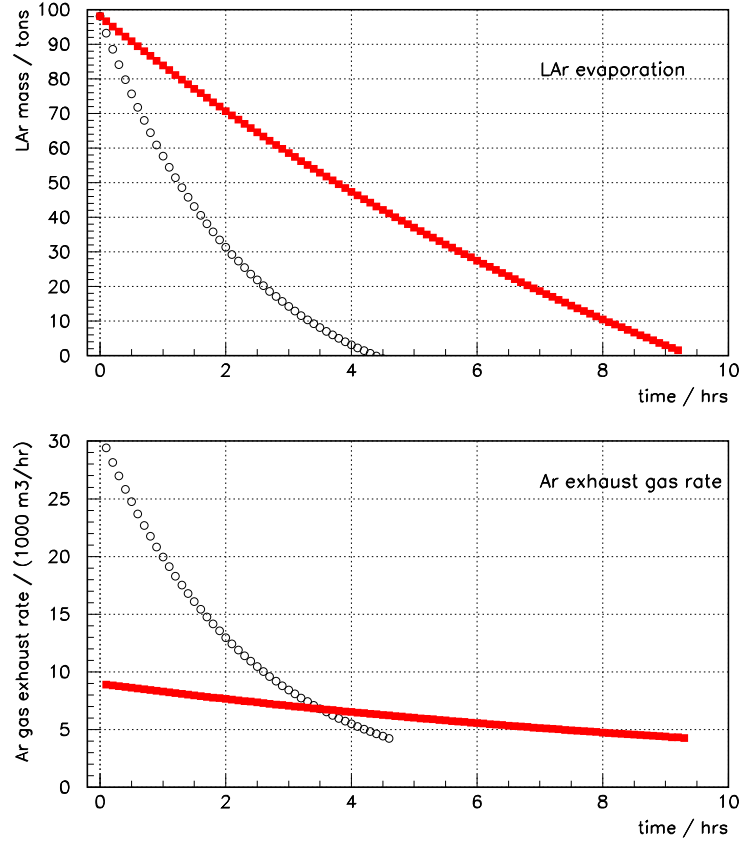


Figure 11. Results of model calculations for the argon mass loss (top) and evaporation rate (bottom) in case of an emergency with a heat transfer coefficient of 27 kW/m² (black open circles) and a reduction to 5 kW/m² in the cylindrical part (red filled circles).

hours to evaporate all LAr, and the gas exhaust rate will stay well below the limit of $10000 \text{ m}^3/\text{hr}$. The limitation of heat transfer can be achieved by covering the wall of the inner vessel with about 5 to 10 mm thick plastic material of thermal conductivity between 0.1 and $0.25 \text{ W}/(\text{m}\cdot\text{K})$. This requirement is well fulfilled by polycarbonat which exhibits also the required vacuum compatibility and low temperature properties. The amount of LAr contained in the volume above the covered cylindrical wall in the vessel head and neck is about 3 m^3 . Its evaporation would take less than 5 minutes in which time the exhaust rate could reach $13000 \text{ m}^3/\text{h}$.

For a leak in the inner vessel similar considerations apply. The maximum gas flow might be lower since overpressure inside the insulation vacuum volume might inhibit further flow of the cryoliquid. However, other than in case of a leak in the outer shell, the prevailing amount of the gas cannot escape through the cryostat's neck but has to pass through the DN100 overpressure release disk mounted on one of the CF200 ports. Thus the insulation volume is also equipped with an overpressure safety device. The thermal shield does not need to be vacuum compatible. Hence on the outside of the outer vessel lightweighted 6 mm thick extruded polystyrol (Jackodur) panels (and a VM2000 foil layer for the muon veto) are used.

5.2 Critical operational parameters, alarms and mitigating actions

Table 5 provides a list of the three COPs identified in the risk analysis [34], (i) pressure in the cryogenic volume of the cryostat, (ii) pressure in the insulation volume, and (iii) the LAr fill level²⁷ in the cryostat's neck. Seven additional COPs allow superior diagnostics of possible failures and the suppression of false alarms: (iv-vi) partial pressures of 'air', argon and water in the insulation vacuum, and four parameters of the water-cooled Ar gas heater, (vii) differential pressure between entrance and exit for the Ar gas being directly proportional to the square of the mass flow through the heater, (viii) temperature of the exhaust gas at its exit, (ix) flow rate of water through heater, and (x) temperature of water at the exit of heat exchanger. All parameters are deduced from at least two redundant sensors except the residual gas pressures and the cooling water parameters. The PLC continously evaluates the COPs, and determines the GERDA safety status in terms of familiar color codes. If some COPs deviate significantly from the foreseen range (see Table 5), it prompts automatically appropriate alarms and actions to mitigate the associated risks.

'Green' indicates standard operation within the specifications. 'Yellow' summarizes all events with no or marginal impact on the safety in hall A indicating the need for corrective maintenance. A typical event for this class would be a loss of insulation vacuum due to an air leak. 'Orange' designates events with little immediate impact on the safety of work in hall A but which might develop to an event of category 'red'. A typical event would be a microscopic leak in one of the cryostat's walls. 'Red' designates the events of highest impact to the complete underground laboratory, e.g. a macrosopic leak in one cryostat wall with the resulting high evaporation rate. The actions for the 'orange' levels 1-3 (see

²⁷This parameter turned out to be irrelevant since an insignificant amount of LAr was lost only during Ge detector immersion.

Table 5. Critical operational parameters (COPs) and thresholds for mitigating actions. The threshold index *code* designates the category of the event which has triggered the respective alarm.

COP		thresholds <i>code</i>			
		green	yellow	orange	red
Cryostat					
p [10^5 Pa _{absolute}]	(i)	< 1.5	> 1.5		
fill level [mm]	(ii)	< -760	> -760		
insulation vacuum					
p [hPa]	(iii)	$< 10^{-4}$		$[10^{-4}, 0.1]_{o3}$	$> 0.1_{r1}$
$p_{res,air}$ [hPa]	(iv)	$< 10^{-4}$	$> 10^{-4}$		
$p_{res,Ar}$ [hPa]	(v)	$< 10^{-4}$		$> 10^{-4}_{o2}$	
$p_{res,water}$ [hPa]	(vi)	$< 10^{-4}$		$> 10^{-4}_{o3}$	
Ar gas heater					
Δp_{Ar} [hPa]	(vii)	< 10		$[10, 30]_{o4}$	$> 30_{r2}$
T_{Ar} [$^{\circ}$ C]	(viii)	> 2		$[-5, 2]_{o5}$	$< -5_{r3}$
\dot{m}_{water} [kg/s]	(ix)	> 5	< 5		
T_{water} [$^{\circ}$ C]	(x)	> 6		$[2, 6]_{o1}$	$< 2_{r4}$

Table 5) include drainage of the water tank, evacuation of hall A, and for o4, o5 and all ‘red’ events in addition increased ventilation in hall A.

Since the filling of cryostat and water tank in 2012 no single red event has shown up. Two alarms in 2017 and 2019 have led to ‘orange’ status. These will be discussed in section 6.3.

6 Commissioning and Performance

6.1 Work at manufacturer

Table 6 shows a summary of the acceptance tests at the manufacturer site in chronological order. In addition, several Rn emanation measurements and cleaning cycles have been made that are discussed below in section 6.2. The maximum operating pressure of $1.5 \cdot 10^5$ Pa rel-

Table 6. Acceptance tests at manufacturer. Pressures quoted for the pressure tests are measured relative to atmospheric pressure. For Rn emanation tests see Table 7.

test	specification / result
pressure test of inner vessel with water	$3.6 \cdot 10^5$ Pa
He leak test of inner vessel	$< 5 \cdot 10^{-9}$ hPa ℓ / s
load test of support pads	passed
He leak test of outer vessel	$< 10^{-7}$ hPa ℓ / s
LN2 evaporation test	< 4 Nm ³ /h or < 300 W
pressure test of outer vessel with N2	$1.85 \cdot 10^5$ Pa

ative to atmospheric pressure ($2.5 \cdot 10^5$ Pa differential with the insulation vacuum present)

for the inner container implies a test pressure of $3.6 \cdot 10^5$ Pa relative to atmospheric pressure. For the outer vessel the test pressure is $1.85 \cdot 10^5$ Pa relative to atmospheric pressure. The pressure test of the inner container was done with water as pressurized medium. The pressure test of the outer container implies, however, the test of the fully assembled cryostat. Hence it was done under appropriate safety precautions with nitrogen gas in order to prevent wetting of the superinsulation. The helium leak tests yielded the requested vacuum performance. Also the pump-down time of about 2 weeks (including purging with dry nitrogen gas) for an insulation vacuum of about 10^{-3} hPa turned out to be acceptable considering the additional polycarbonate layer below the MLI.

The inner vessel rests on 8 support pads. To ensure that all pads carry about equal load, a special test was carried out: by temporarily mounting on each support pad a load cell, the weight on each pad was measured after the empty inner vessel had been lowered onto the pads. With each pad resting on a Belleville spring of known spring constant (58 kN/mm), the differences between the measured loads translated into length differences of less than 0.12 mm.

The evaporation rate of the cryostat has been determined with a fill of LN2 up to the neck at an insulation vacuum of 10^{-3} hPa. During cool down, temperatures were monitored at various locations of the cryostat by sensors installed either below the MLI at the bottom and top of the vertical wall of the inner vessel or mounted with appropriate thermal insulation on the vertical filling pipe inside the cryostat. LN2 was distributed within the cryostat by a sprinkler with small holes covering a large surface and avoiding a cold spot. The flow of LN2 was adjusted such that the cooling speed was less than 20 K/h and the maximum temperature difference among all sensors less than 50 K. A few hours after the completion of the fill, the spillway valve was closed, and the emerging gas was let via a bundle of ambient air heat exchanger columns to a GN2 flow meter. Fig. 12 shows the measured evaporation rate during the settling time until equilibrium. The asymptotic flow of nitrogen is well below the specified rate of 4 m³/h and corresponds to a thermal loss of less than 300 W.

6.2 Work in hall A of LNGS

The cryostat was transported in horizontal orientation by flat bed truck to LNGS. A metal rod inserted between top flange and bottom of the inner vessel prevented any horizontal movement of the inner vessel. After arrival and erection in hall A the evaporation rate of the cryostat was measured again, and the previously measured result was reproduced.

Installation of internal copper shield

The installation of the copper shield proceeded from a platform built around the cryostat's neck. A tent with an inside hoist was erected above the neck opening and kept at slight overpressure to limit the amount of dust entering the cryostat. The individual copper segments were brought with the hall crane up to the platform and transferred into the tent after removal of the outer plastic cover. The segments were lowered with the hoist into the cryostat, freed there from the second plastic cover, and picked up by a temporarily installed handling device that allowed to mount them at the appropriate location.

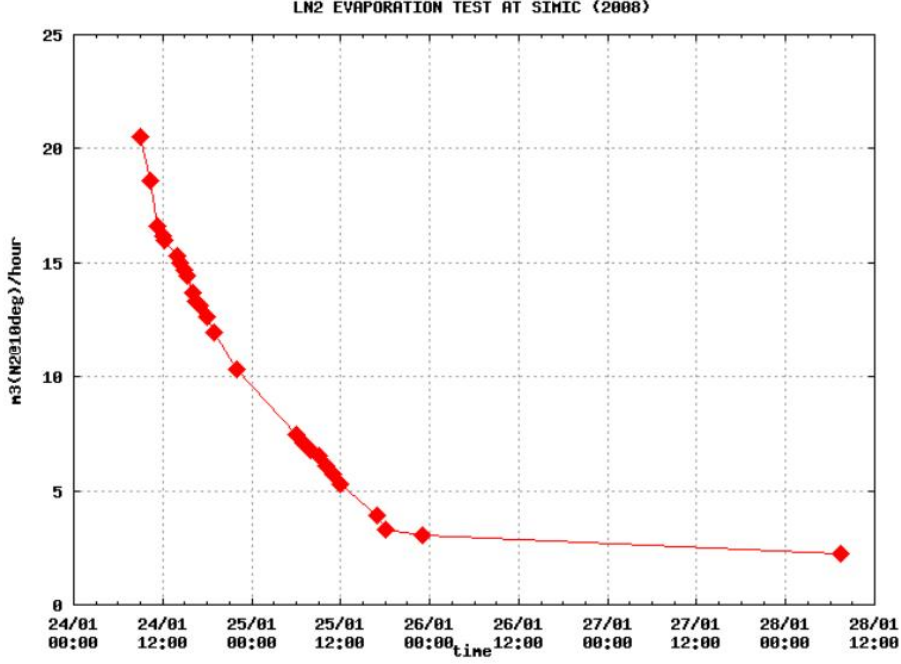


Figure 12. Settling of evaporation rate after LN2 fill.

Radon emanation tests

A crucial specification of the cryostat is its radon emanation. Monte Carlo studies indicate that a homogeneous distribution of 8 mBq of ^{222}Rn within the inner vessel would add 10^{-4} cts/(keV·kg·yr) to the background index.

The emanation measurements were performed with the mobile extraction unit (MOREX) [35]. For each run the inner vessel was closed with a metal-sealed steel flange. In order to remove air-borne ^{222}Rn the vessel was evacuated and filled twice with ^{222}Rn -free nitrogen gas that was purified during the fill with the cryogenic activated carbon traps of MOREX. The vessel was pressurized then up to $1.6 \cdot 10^5$ Pa relative to atmospheric pressure and subsequently closed to accumulate the emanating ^{222}Rn . After 1 to 2 weeks the gas was mixed within the vessel to establish a homogeneous ^{222}Rn distribution, and at least two gas fractions of typical 20 to 40 m³ were extracted for the determination of their respective ^{222}Rn concentration. Scaling these data to the total volume yielded then the total saturation emanation rates.

Table 7 shows the various emanation rates that have been determined at various phases of the commissioning of the cryostat. Two extractions after the first cleaning cycle of pickling, passivation and rinsing with de-ionized water yielded rather different values, possibly due to a fractioning of Rn inside the vessel such that the heavier Rn is concentrated at the bottom. Hence the Rn concentration is enhanced in the second sample. Moreover, it was noted that the cryostat's inner surface was not everywhere metallic bright after the first

Table 7. ^{222}Rn emanation in GERDA cryostat. Quoted results are the average of at least two extractions, uncertainties include both statistical and systematic contributions.

Test	Activity [mBq]	Comment
1	23.3 ± 3.6	cryostat after cleaning
2a	13.6 ± 2.5	after additional cleaning
2b	13.7 ± 2.8	
3	34.4 ± 6.0	after Cu shield mounting
4	30.6 ± 2.4	after wiping of inner surfaces
5	54.7 ± 3.5	after mounting of infrastructure

cleaning. Hence grinding at various spots and another cleaning cycle were done, and in the subsequent emanation measurement the gas was mixed before the extraction of samples, one at the manufacturer’s site and one after transport to LNGS. Two consistent and significantly lower values were measured which, considering the volume, compare very well with values measured for other selected cryogenic vessels. After the mounting of the internal copper shield the emanation rate showed an unexpected large increase. Subsequent wiping of all accessible steel and copper surfaces did barely improve the more precisely measured emanation value of about 31 mBq which is more than twice the value of the empty vessel. Later screening of the copper material revealed a surface contamination which presumably was not removed by the acid treatment at the rolling mill. The installation of the cryogenic infrastructure further increased the emanation level by almost a factor of two. The measurements indicate that the new sources could be located in the pipes above the cryostat.

During data taking we did not detect a high radon level inside the liquid argon with the germanium detectors. This indicates that the radon emanating from the piping does not mix with the argon.

Final installation work

Work close to the cryostat included the construction of the surrounding water tank and the infrastructure building for GERDA with the platform above the cryostat for cleanroom and lock. Latter activities caused the occasional deposition of carbon steel debris on some unprotected surfaces of the cryostat. When noticed, protection measures were improved, and after the end of the construction work the surface of the cryostat was carefully inspected. All spots showing carbon steel deposits were grinded, pickled and passivated. These activities as well as the installation of the Jackodur thermal insulation took advantage of the scaffolding that was available within the water tank for covering the inner walls of the water tank with the reflecting VM2000 foil.

With platform and cleanroom available, heat exchanger and radon shroud were inserted under controlled clean conditions into the cryostat. With the manifold mounted the internal instrumentation of the cryostat was connected to the outside cryogenic infras-

structure including an ullage volume of 2.6 m^3 . Connections of pipes were kept short by locating the latter close to the wall of the water tanks with the exception of the LN2 and LAr storage tanks. The installation concluded by connecting the big DN630 shutter in the cleanroom via a double-walled bellow to the top of the manifold.

6.3 Performance and operating experience

Initially, the insulation vacuum was pumped at a pressure drop of $1 - 2\text{ Pa/s}$ to avoid damage to the superinsulation. Once the pressure was below 1 hPa a turbo pump was switched on and after two month of pumping a pressure of 10^{-5} hPa was reached and the cryostat was filled. After cool down the pressure dropped to about $2 \cdot 10^{-8}\text{ hPa}$. The turbo pump is running continuously. If it is switched off, the vacuum pressure increases at $5 \cdot 10^{-7}\text{ hPa}\cdot\ell/\text{sec}$.

Inspection for corrosion after GERDA Phase I

After more than 3 years of operation the water tank was drained in July 2013. The cryostat's outer thermal insulation (Jackodur covered by VM2000 foil) appeared to be in perfect condition. Selected welds and surfaces of water tank and cryostat were inspected by a representative of a notified body (INAIL, P.le Pastore 6, 00144 Roma). No corrosion problems were observed (including surfaces below the thermal shield), and the safety of the pressure equipment was certified. Subsequently, the water tank was refilled and kept with two interruptions (see below) at its final level since September 2013.

Unscheduled drainage of water tank

Two alarms related to the insulation vacuum pressure triggered the drainage of the water tank during the 12 years of operation. In the first event (15/04/2017) one of the two pressure gauges was broken. The PLC recognized this condition and disabled the sensor for alarm generation. By human intervention, the faulty sensor was mistakenly enabled again and soon afterwards the alarm threshold was passed which triggered the drainage. We decided to have shorter maintenance intervals in order to reduce the risk of a sensor failure in the future.

The second event (11/11/2019) was triggered by a broken turbo pump such that the vacuum pressure increased within hours above the alarm threshold. The PLC closed the gate valve and separated the insulation vacuum from the pump. The cold cryostat wall then acted as a cryopump and the insulation vacuum pressure quickly returned below the threshold. The drainage however was started and had to be stopped manually.

We are discussing with LNGS to modify the alarm and drainage conditions to reduce the risk of false alarms without jeopardizing the safety of the system.

Both events provided, however, evidence for the full functionality of the implemented safety system.

Drainage of LAr

After completion of all GERDA measurements, the water tank and thereafter the cryostat were emptied. The drainage of the LAr occurred by evaporation. It started in September

2020 by increasing the insulation vacuum pressure to about 1 hPa and later in steps to 5 hPa and 30 hPa. Hence the heat transfer from the outside to the inner steel vessel the LAr increased. We did not go higher in pressure since the expectation is that the heat transfer actually reduces at some point when going higher in pressure, and we also did not want to harm the MLI of the cryostat. The evaporation of the 90 tons of LAr took about 7 weeks, longer than we expected from previous experience with LN2.

The cryostat was filled twice with LN2 at the time of production as part of the acceptance test. The evaporation rate at that time was much higher: emptying the cryostat took typically 2 weeks. We think the reason why it took much longer now is due to a) the larger heat to evaporate the 90 tons of argon compared to the 52 tons of nitrogen (40%), b) the additional thermal insulation on the outside of the outer cryostat wall (5 mm of extruded polystyrol foam and the VM1000 reflector foil), and c) the reduced air volume inside the water tank.

Inspection of the cryostat after GERDA Phase II

In November 2020, i.e. 11 years after the LAr fill, an optical inspection of the cryostat has been performed both from the outside and inside. No damage or deformation was observed. Moreover, cryostat and infrastructure passed without problem the required tests according to Italian regulations.

7 Conclusion

The GERDA experiment is the first realization of a novel shielding scheme using a cryostat filled with a liquid noble gas that is operated in a large water tank, a concept that has since been adopted by other experiments like LUX [14], XENON1t [15], Darkside [16], or PandaX-4T [17]. The associated risks have been carefully analysed and mitigated. The major construction materials of the cryostat have been all screened for radioactivity. The cryogenic installation is running since December 2009 without any problem that would have affected safety. The background goals for GERDA have been reached demonstrating the feasibility of a background-free $0\nu\beta\beta$ decay experiment with ^{76}Ge at the design exposure of 100 kg·yr [7]. The experimental setup of GERDA has been handed over in February 2020 to the LEGEND collaboration [18] which is preparing the next generation search for $0\nu\beta\beta$ decay of ^{76}Ge using thereby major parts of the GERDA experimental setup including water tank and cryostat with its infrastructure.

Acknowledgments

The authors gratefully acknowledge the generous and most helpful support by Ch. Haberstroh, H. Neumann and G. Perinic in numerous cryogenic issues. We acknowledge also the help of V.N. Cryshtal and E.A. Bogdanov (Cryogenmash) in the design studies for a superinsulated stainless steel cryostat with internal cold copper shielding. We thank our referees for critically reading the manuscript and suggesting substantial improvements.

This work was supported by special funds of the Max Planck Society (MPG).

A Heat transfer to LN2 and LAr in the pool boiling regime

Studies of the gas exhaust rate for a worst case failure scenario of the GERDA cryostat have been performed on a small scale model. The experimental setup consisted of two concentric cylindrical containers of about 50 cm height, an inner one ($\varnothing 30$ cm) from stainless steel for the cryoliquid, and an outer one ($\varnothing 50$ cm) for the water. The inner container is resting on plastic feet for thermal insulation. The weight of both containers including the reservoir containing the water is continuously monitored with a digital scale whose display is quasi-continuously read with a camcorder. Temperatures were measured with Pt100 sensors mounted within 1 mm at the outer surface of the wall of the inner container as well as at 10 mm and 20 mm distance from it.

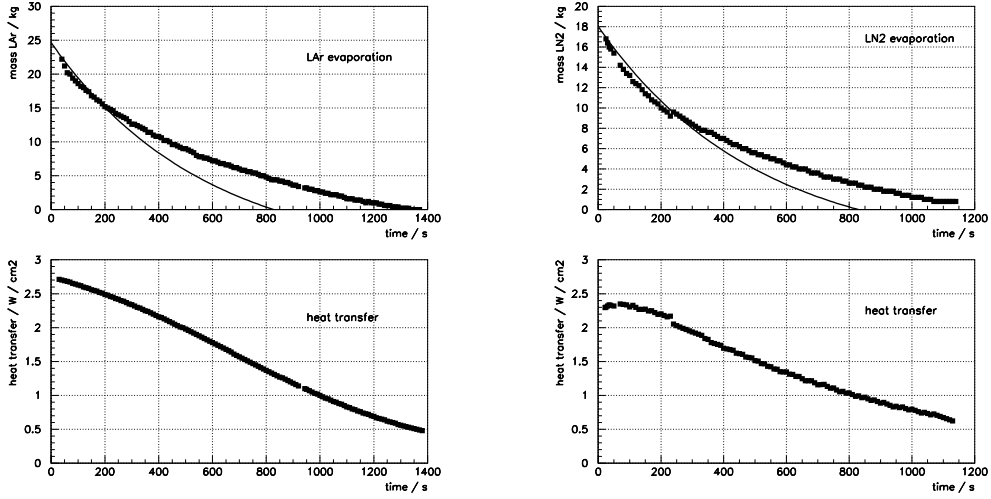


Figure 13. (top) Time dependence of the LN2 and LAr mass after exposure of the container containing the cryoliquid to the water bath. The continuous lines are calculated with the integral of eq. (1) using a heat transfer coefficient of 24 kW/m^2 for LN2, and 27 kW/m^2 for LAr. (bottom) Time dependence of the heat transfer coefficients deduced with eq. (1) from the data shown on top.

Fig. 13 shows the results obtained for LN2 and LAr. Data points obtained during the sudden filling and in the following 20 sec time interval are not shown since the setup was not adequate to map out these highly transient processes. Corresponding heat transfer coefficients k were deduced using the relation

$$\frac{dM}{dt} = - \frac{k \cdot \pi \cdot R^2}{h} - \frac{2 \cdot k}{\rho \cdot R \cdot h} \cdot M \quad (1)$$

where M , ρ and h denote mass, density and latent heat of the cryoliquid in the container of radius R ($h = 162$ kJ/kg and 199 kJ/kg for LAr and LN2, respectively). The heat transfer coefficients decrease with time and we adopt as k value the maximum of 24 kW/m² and 27 kW/m² for LN2 and LAr, respectively. The k value for LN2 is close to the expectation from the pool boiling characteristics of LN2 [32]. For LAr, we are not aware of published values. The deduced k values represent an upper limit since it is assumed that the surface covered by the cryogenic liquid is minimal at all times. This assumption neglects the well visible effect that the boiling liquid wells up the wall.

One reason for the decreasing heat transfer coefficients is the built up of an ice layer at the wall of the inner container. With a thermal conductivity of ice of about $3\text{W}/(\text{m}\cdot\text{K})$ the corresponding heat transfer coefficient for a layer of 20 mm thickness and $\Delta T = 100$ K is $15\text{ kW}/\text{m}^2$ limiting thus the effective heat flow. The temperature measurements performed with LAr show that the ice thickness of 10 mm and 20 mm is reached after about 300 and 600 seconds.

B Timeline of the GERDA experiment

Table 8. Timeline of the GERDA experiment.

Event	Date
Letter of Intent to LNGS	Apr. 2004
Proposal to LNGS	Sep. 2004
Technical Proposal	June 2006
Risc Analysis finalized	Feb. 2007
Arrival of cryostat at LNGS	Mar. 2008
Cryostat and water tank installed	June 2008
L'Aquila earthquake	Apr. 2009
Cryostat filled with LAr	Dec. 2009
First detectors deployed in LAr	June 2010
Data taking Phase I	Nov. 2011 - May 2013
Upgrade to Phase II	June 2013 - Nov.2015
Data taking Phase II	Dec. 2015 - May 2018
Data taking Phase II	July 2018 - Dec.2019
GERDA setup handed over to LEGEND-200	Feb. 2020

References

- [1] K.-H. Ackermann et al. [GERDA collaboration], *The GERDA experiment for the search of $0\nu\beta\beta$ decay in ^{76}Ge* , *Eur. Phys. J. C* **73** (2013) 2330.
- [2] M. Agostini et al. [GERDA collaboration], *Results on Neutrinoless Double- β Decay of ^{76}Ge from Phase I of the GERDA Experiment*, *Phys. Rev. Lett.* **111** (2013) 122503.
- [3] M. Agostini et al. [GERDA collaboration], *Upgrade for Phase II of the GERDA Experiment*, *Eur. Phys. J. C* **78** (2018) 388.

- [4] M. Agostini et al. [GERDA collaboration], *Background-free search for neutrinoless double- β decay of ^{76}Ge with GERDA*, *Nature* **544** (2017) 47
arXiv:1703.00570.
- [5] M. Agostini et al. [GERDA collaboration], *Improved Limit on Neutrinoless Double- β decay of ^{76}Ge from GERDA Phase II*, *Phys. Rev. Lett.* **120** (2018) 132503
arXiv:1803.11100.
- [6] M. Agostini et al. [GERDA collaboration], *Probing Majorana neutrinos with double- β decay*, *Science* **365** (2019) 1445; published online 05 Sep 2019
DOI:10.1126/science.aav8613.
- [7] M. Agostini et al. [GERDA collaboration], *Final Results of GERDA on the Search for Neutrinoless Double- β Decay*, *Phys. Rev. Lett.* **125** (2020) 252502.
- [8] S. Davidson, E. Nardi, and Y. Nir, *Leptogenesis*, *Phys. Rep.* **466** (2008) 105.
- [9] I. Abt et al., *A New Ge Double Beta Decay Experiment at LNGS*, Letter of Intent, 16 March 2004, arXiv:hep-ex/0404039v1 29 Apr 2004.
- [10] E. Fiorini, A. Pullia, G. Bertolini, F. Cappellani and G. Restelli, *A Search for Lepton Nonconservation in Double Beta Decay with a Germanium Detector*, *Phys. Lett.* **25B** (1967) 602.
- [11] G. Heusser, *Low-Radioactivity Background Techniques*, *Ann. Rev. Nucl. Part. Sci.* **45** (1995) 543.
- [12] Yu.G. Zdesenko, O.A. Ponkratenko, V.I. Tretyak, *High sensitivity GEM experiment on 2β decay of ^{76}Ge* , *J. Phys. G: Nucl. Part. Phys.* **27** (2001) 2129
[nucl-ex/0106021].
- [13] K. Freund et al., *The performance of the Muon Veto of the GERDA experiment*, *Eur. Phys. J. C* **76** (2016) 298.
- [14] D. Akerib et al., *The Large Underground Xenon (LUX) experiment*, *Nucl. Instr. Methods A* **704** (2013) 111.
- [15] E. Aprile et al., *The XENON1T dark matter experiment*, *Eur. Phys. J. C* **77** (2017) 881.
- [16] C.E. Aalseth et al., *The DarkSide Multiton Detector for the Direct Dark Matter Search*, *Adv. High Energy Physics* **2015** Article ID 541362, 8 pages
<http://dx.doi.org/10.1155/2015/541362>.
- [17] H. Zhang, A. Abdukerim, W. Chen et al., *Dark matter direct search sensitivity of the PandaX-4T experiment*, *Sci. China Phys. Mech. Astron.* **62** (2019) 31011
<https://doi.org/10.1007/s11433-018-9259-0>.
- [18] N. Abgrall et al., *The large enriched germanium experiment for neutrinoless double beta decay (LEGEND)*, *AIP Conf. Proc.* **1894** (2017) 020027.
- [19] I. Abt et al. [GERDA collaboration], *Gerda - The GERmanium Detector Array for the search of neutrinoless $\beta\beta$ decay of ^{76}Ge at LNGS*, Proposal to the LNGS P38/04, September 2004
<http://www.mpi-hd.mpg.de/gerda/proposal>.
- [20] O. Chkvorets, *Search for double beta decay with HPGe detectors at the Gran Sasso underground laboratory*, Ph.D. thesis, Heidelberg 2008
<http://www.ub.uni-heidelberg.de/archiv/8572>.

- [21] I. Barabanov et al., *Shielding of the GERDA experiment against external gamma background*, *Nucl. Instrum. Methods A* **606** (2009) 790.
- [22] J. de Wit, *EEMUA recommendations for the design and construction of refrigerated liquefied gas storage tanks*, *Cryogenics* **28** (1988) 800.
- [23] W.H. Aitken and P.H. Hanish, *Design of inner containment tanks for liquid oxygen and liquid nitrogen*, *Cryogenics* **28** (1988) 805.
- [24] R. Tartaglia and A. Giampaoli *Safety Guide for the experiments at the Laboratori Nazionali del Gran Sasso* INFN, Servizio Prevenzione e Protezione (2002).
- [25] IAEA, *Applicability of the leak before break concept*, Vienna, IAEA-TECDOC-710 (1993).
- [26] W. Maneschg, M. Laubenstein, D. Budjas, W. Hampel, G. Heusser, K.T. Knöpfle, B. Schwingenheuer, and H. Simgen, *Measurements of extremely low radioactivity levels in stainless steel for GERDA*, *Nucl. Instr. Methods A* **593** (2008) 448.
- [27] M. Barucci, E. Olivieri, E. Pasca, L. Risegari, and G. Ventura, *Thermal conductivity of Torlon between 4.2 and 300 K*, *Cryogenics* **45** (2005) 295.
- [28] <http://content.solvay.com/torlon-pai-design-guide>.
- [29] Ch. Haberstroh, *Cryogenic Supply for the GERDA Experiment*, *Advances in Cryogenic Engineering* **53** (2007) 1201.
- [30] R. Brugnera, F. Costa, A. Garfagnini, G. Gigante, S. Hemmer, I. Lippi, M. Michelotto, C. Urb, and D. Zinato, *The slow control system of the GERDA double beta decay experiment at Gran Sasso, 2012 JINST* **7** P10017.
- [31] K.D. Timmerhaus and Th.M. Flynn, *Cryogenic Process Engineering*, Plenum Press, 1989, ISBN 0-306-43283-8.
- [32] R.W. Vance, *Cryogenic Engineering*, John Wiley & Sons, Inc., New York, London.
- [33] W.G. Fastowski, J.W. Petrowski, A.E. Rowinski, *Kryotechnik*, Akademie-Verlag, Berlin 1970.
- [34] NIER Ingegneria S.p.A., *Cryogenic and Water Tank System, Preliminary Risk Analysis (final version)*, Bologna 2017.
- [35] G. Heusser, W. Rau, B. Freudiger, M. Laubenstein, M. Balata, T. Kirsten, *^{222}Rn detection at the $\mu\text{Bq}/\text{m}^3$ range in nitrogen gas and a new Rn purification technique for liquid nitrogen*, *Appl. Rad. Isot.* **52** (2000) 691.